Optik 156 (2018) 635–645

Contents lists available at ScienceDirect

Optik

journal homepage: www.elsevier.de/ijleo

Design of angle-resolved illumination optics using nonimaging bi-telecentricity for 193 nm scatterfield microscopy

Martin Y. Sohn*, Bryan M. Barnes, Richard M. Silver

Engineering Physics Division, National Institute of Standards and Technology, 100 Bureau Drive, Gaithersburg, MD 20899, USA

ARTICLE INFO

Article history:
Received 29 March 2017
Received in revised form
28 November 2017
Accepted 29 November 2017

Keywords:
Optical microscopy
Scatterfield microscopy
Lens system design
Angle-resolved illumination
Bi-telecentric system
193 nm microscopy

ABSTRACT

Accurate optics-based dimensional measurements of features sized well-below the diffraction limit require a thorough understanding of the illumination within the optical column and of the three-dimensional scattered fields that contain the information required for quantitative metrology. Scatterfield microscopy can pair simulations with angle-resolved tool characterization to improve agreement between the experiment and calculated libraries, yielding sub-nanometer parametric uncertainties. Optimized angle-resolved illumination requires bi-telecentric optics in which a telecentric sample plane defined by a Köhler illumination configuration and a telecentric conjugate back focal plane (CBFP) of the objective lens; scanning an aperture or an aperture source at the CBFP allows control of the illumination beam angle at the sample plane with minimal distortion. A bi-telecentric illumination optics have been designed enabling angle-resolved illumination for both aperture and source scanning modes while yielding low distortion and chief ray parallelism. The optimized design features a maximum chief ray angle at the CBFP of 0.002° and maximum wavefront deviations of less than 0.06 λ for angle-resolved illumination beams at the sample plane, holding promise for high quality angle-resolved illumination for improved measurements of deep-subwavelength structures using deep-ultraviolet light.

1. Introduction

In optical microscopy, information about the shapes and dimensions of features is contained in the scattered fields created as these features are illuminated, even when their sizes are well below the diffraction limit and thus are unresolved. By engineering these three-dimensional scattered fields within a high magnification imaging microscope, the scatterfield microscopy technique optimizes measurements of nanoscale dimensions which can be determined by comparing the measured intensities against libraries of electromagnetic scattering simulations generated using parametric geometry models [1–4]. In a recent study, three-dimensional nanostructures were quantified utilizing a visible microscope optics by reconstructing the scattered fields from multiple defocused images utilizing a visible microscope optics as these images contain phase and spatial frequency information [5]. Proper design, implementation, and characterization of the microscope tool using angle-resolved illumination are essential as compensations to the simulated scattered fields are required in this technique to allow comparisons between experimentally measured intensities and theoretically simulated intensities that

* Corresponding author.
E-mail address: martin.sohn@nist.gov (M.Y. Sohn).

https://doi.org/10.1016/j.ijleo.2017.11.206
0030-4026/

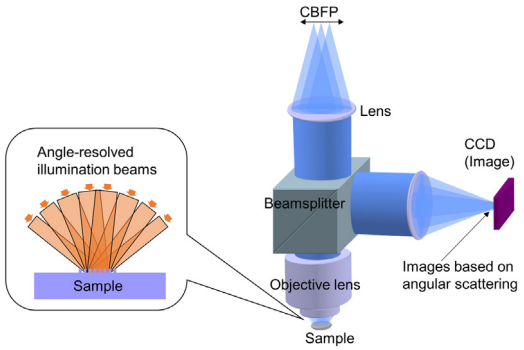

Fig. 1. Schematic diagram of angle-resolved scatterfield microscopy.

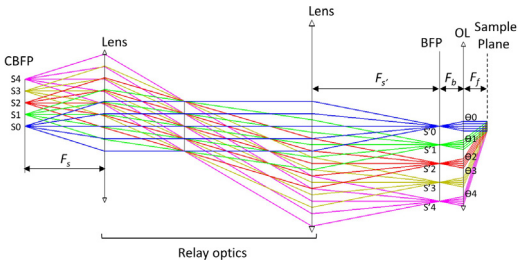

Fig. 2. Schematic diagram of bi-telecentric optics for angle-resolved illumination.

assume an ideal microscope model. This scatterfield microscopy technique may address the growing demand of optical measurement capabilities for nanoscale features and defects beyond the diffraction limit in semiconductor fabrication process control with high accuracy and low uncertainty [5–8].

In scatterfield microscopy, angular control of the illumination is the key to tailoring the scattered fields efficiently. Manipulation of the angle of the illumination beam is achieved by implementing a conjugate to the back focal plane (CBFP) of an objective lens in a Köhler illumination optics, at which the illumination beam at the sample plane can be modified as shown in Fig. 1. Discretely scanning the CBFP area using an aperture produces controlled angle-resolved illumination beams as the CBFP can be considered as a series of point sources that yield plane waves at the sample plane. The scattered intensity profiles at the image plane are analyzed based on characterizing the optical paths using the angle-resolved illumination beams generated by scanning this aperture. Engineering of the illumination beam at the sample plane from the CBFP is bounded by the proper design of the illumination optics [3,5,9,10].

For the majority of conventional microscope optical systems with Köhler illumination, the CBFP space is non-telecentric while the sample plane space is telecentric, as the primary consideration is to establish a homogeneous lateral intensity distribution in the illumination at the sample plane, which does not require telecentricity in the CBFP surface [11–14]. However, making the CBFP telecentric allows for low distortion in the transformation between the CBFP spots and the angle-resolved illumination beams, which quantitatively yields even wavefronts as a function of the illumination angle [15]. Telecentricity also yields parallelism between the chief rays of the beams diverging from the CBFP, which allows not only scanning an aperture but also the direct access of a beam source to the CBFP as an additional method to yield angle-resolved illumination beams [16–18]. These benefits of telecentric CBFP increase the performance of an illumination optics system using a shorter wavelength, such as the deep ultraviolet (DUV) range for higher resolution scatterfield imaging. This paper describes the design procedure and evaluations required to implement a bi-telecentric Köhler illumination optics for generating angle-resolved illumination beams for a reflection scatterfield microscope operating at a wavelength of 193 nm.

2. Nonimaging bi-telecentric illumination optics

Unlike most conventional bi-telecentric optical systems, in which points in the object plane are transformed into points in the image plane, a bi-telecentric system for angle-resolved illumination transforms points in the object plane to collimated beams at the sample plane [17–21] as a nonimaging optics. As shown in Fig. 2, the beams diverging from the points, S, in the CBFP as an object space, in which chief rays are parallel, become the collimated beams converging to the sample plane through the back focal plane (BFP). The angular illumination beams are thus governed by a conversion relationship between the position of the CBFP points and the incident angle at the sample plane. Assuming bi-telecentric optics within a Köhler illumination configuration, diverging beams coming out of these points at the CBFP propagate to the sample plane

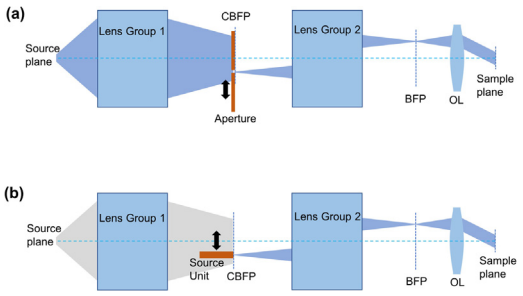

Fig. 3. Two methods of angle-resolved illumination using beam scanning at CBFP: (a) aperture scan method and (b) source module scan method.

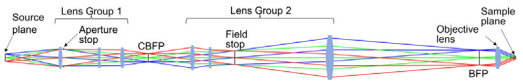

Fig. 4. Schematic diagram of angle-resolved microscope illumination optics.

as angularly collimated beams through the Relay optics and the objective lens (OL). The relationship of the linear position, S, in the CBFP to the illumination angle, θ, is expressed as Eq. (1),

$$\theta = arcsin\frac{1}{\sqrt{(F_f/(M \cdot S))^2}} \tag{1}$$

where, F_f is the front focal length of the OL and M is the magnification between the CBFP and the BFP. The magnification is defined as $= F_{s'}/F_s$, where F_s and $F_{s'}$ are the focal lengths of the relay optics. The relay optics transferring the CBFP image to the BFP requires high magnification to increase the angular resolution of the illumination beam for a given objective lens while maintaining appropriately low aberrations.

This bi-telecentric illumination configuration enables two separate engineering methods at the CBFP as shown in Fig. 3: (a) the aperture scan method and (b) the source scan method. For the aperture scan method, the whole microscope illumination optics including Lens Group 1 and 2 is utilized and a small aperture is positioned at the CBFP to form an angular illumination beam at the sample plane. For the source scan method, only Lens Group 2 between the CBFP and the BFP is engaged and Lens Group 1 is replaced with a source unit which can be a fiber end, a laser diode, or an optic to generate a laterally scanning beam. Both cases require high telecentricity of the CBFP for obtaining low distortion of the collimated beam transformed from the aperture spot as well as maintaining a near constant relationship between CBFP position and illumination angle across the CBFP area. The capabilities to implement either one of these dual options as enabled by a bi-telecentric system is a primary consideration of the optics design criteria.

3. Design criteria for angle-resolved illumination optics

The design should establish a bi-telecentric optics transforming beams diverging from a telecentric CBFP to angle-resolved collimated beams at the sample plane utilizing a Köhler illumination configuration. Fig. 4 schematically illustrates the basic structure of the illumination optics showing critical planes essential to produce angle-resolved illumination. The key conjugate planes are the source plane, the CBFP, and the back focal plane (BFP) of the objective lens (OL) in front of the sample plane. Lens Group 1 relays between the source plane and the CBFP to form a telecentric CBFP surface, while Lens Group 2 transforms the points in the CBFP to the angular collimated beams at the sample plane through the BFP [22].

There are three main goals for the design of an effective angle-resolved illumination optics. First, both the CBFP and the sample plane must have a high telecentricity to reduce deviations in the conversion relationship between CBFP position and the illumination angle. Second, the CBFP must be large enough to be resolved by physical components such as an aperture, a source aperture, or a spatially projected scanning spot while preserving this high telecentricity. The challenge is that the CBFP diameter is linked to its NA and the diameter must be balanced between the optimization of angular resolution and the energy fluence minimization of this balance arises as the diameter is inversely proportional to the NA while the energy fluence is proportional to the NA which is related to the source NA and its diameter. Considering these relationships, the CBFP diameter targeted to be larger than 10 mm in diameter for appropriate angle resolution. Third, the angle-resolved illumination beams must have low wavefront distortion throughout the range of the illumination angles. This consideration secures that the scattered fields can be assessed using the electromagnetic scattering simulation.

In order to design specific lenses and spaces from that will yield an efficient angle-resolved bi-telecentric illumination optics operating with an excimer laser at 193 nm wavelength, there are some key design constraints as specified in Table 1. An overarching concern at this wavelength is that the flux density of the beam passing through the optical components must be minimized to avoid damage due to the high energy of the excimer laser light [23]. The beam passing throughout

Table 1
Optics design constraints for 193 nm angle-resolved bi-telecentric illumination optics.

Major constraints	Specific metrics	Values
Energy fluence	Damage threshold	1.0 J/cm^2
Objective lens	Maximum NA	0.12–0.74
	Working distance	~8 mm
	Effective front focal length	2.6 mm
	Entrance NA	0.022
	BFP diameter	~4 mm
Illumination optics	Source diameter	>3 mm
	CBFP diameter	>10 mm
	Field stop diameter	>10 mm
	Field of view (FOV) diameter	>30 μm
Aberrations	Telecentric CBFP:	
	Chief ray angle deviation	<0.01°
	Field distortion	<0.1%
	Telecentric sample plane:	
	RMS wavefront error	≤λ/14 (0.071 λ)

the optical paths must be shaped to avoid any high concentration area as this would result in solarization of the coating materials or generation of plasma between optical components, assuming that a damage threshold of the coating layers is 1.0 J/cm^2.

One major prior constraint is the objective lens which governs the numerical apertures (NAs) and diameters of the key planes according to the conservation of ray flux [24]. Specifically, the design uses a commercial catadioptric objective lens for a wavelength of 193 nm with an NA 0.74 with an obscuration of NA 0.12, an effective focal length of 2.6 mm, and a working distance of about 8 mm as shown in Table 1. It also yields a back focal plane (BFP) with a diameter of 4 mm and an entrance NA of 0.022. The illumination optics needs to be designed about these key, established unalterable constraints predefined by the objective lens.

Major surfaces of the illumination optics such as the source plane, the CBFP, the field plane, and the sample plane are to be enlarged within the other constraints to have relatively large size for angle scanning with enough resolution. Here, diameters of the CBFP and the Field Stop must be more than 10 mm to have flexibility and scanning resolution. A field of view (FOV) diameter of about 30 μm is determined by an image magnification and the diagonal length of image CCD in collection optics, at which the scattered light is imaged.

Aberrations are considered for two major surfaces, a telecentric CBFP and a telecentric sample plane, to yield telecentricity and wavefront homogeneity. Maximum chief ray angle deviation and field distortion at the CBFP must be less than 0.01° and 0.1% over the surface area to be a qualified telecentric CBFP surface [15]. Angle-resolved beams at the sample plane configured with a Kohler illumination configuration must have a maximum wavefront error of less than λ/14 (0.071 λ) to meet the Maréchal criterion by which the limit of error of a diffraction limited system is defined [25–27].

Under these criteria, the illumination optics are designed based on a bi-telecentric CBFP large enough to angularly resolve the illumination beam cone at the sample plane.

4. Design and optimization

Fig. 5 shows the design flow for optimizing the optics for angle-resolved illumination. As the first step, a global structure of the two Lens Groups is designed with lens parameters such as thickness, curvatures, distances set to form a CBFP with a minimum diameter of 10 mm while maintaining the entrance NA of the OL of 0.022 and a source diameter of 3 mm. Based on the global optics, Lens Group 2 is designed initially in the reverse direction, starting at the sample plane to produce a telecentric CBFP through an appropriate field stop, and then Lens Group 1 is designed with respect to the CBFP in the forward direction to fit for the CBFP diameter and NA formed by Lens Group 2. Once the two Lens Groups are initially designed, matching between the two and fine optimization is performed to determine the CBFP NA and its diameter with acceptable telecentricity and aberrations. The parameters of these 12 lenses are adjusted iteratively with consideration for the energy fluence and the aberrations while optimizing for the NA and diameter of the CBFP.

In the fine adjustments of these two Lens Groups, the individual lens surfaces are adjusted along the distances between the surfaces to form an appropriate telecentric CBFP and non-imaging sample plane.

The complete design and optimization involve six lenses placed within the two Lens Groups that are formed to obtain a telecentric CBFP with optimized NA and diameter as shown in Fig. 6. Curvatures and distances of the two lens groups consisting of triplets (L11, L21), singlets (L12, L22), and doublets (L13, L23) are optimized following the design flow in Fig. 5. The distance pairs, a_{11}, a_{12} and a_{21}, a_{22} are determined by magnifications of the two lens groups to match them with respect to the CBFP. The distances l_{11}, l_{12}, l_{21}, and l_{22} are the key parameters used for fine adjustment of NA and diameter at the CBFP with adjustments of the lenses.

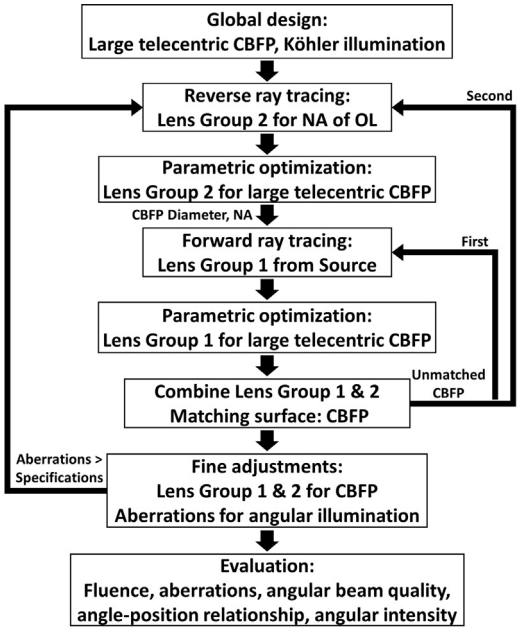

Fig. 5. Design flow for angle-resolved illumination optics.

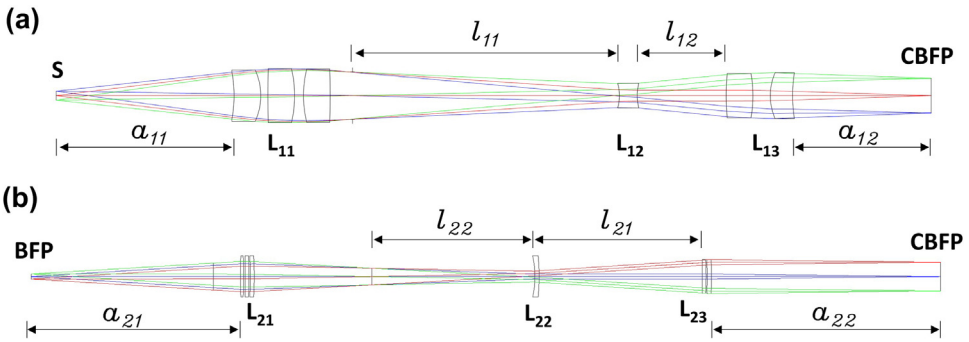

Fig. 6. Lens combinations for optimization: (a) Lens group 1 and (b) Lens group 2. L_{11}, L_{21}: triplet, L_{12}, L_{21} singlet, L_{13}, L_{23}: doublet, a_{11}, a_{12}, a_{21}, a_{22}: distance to critical surfaces, l_{11}, l_{12}, l_{22}, l_{21}: critical parameters for fine adjustment.

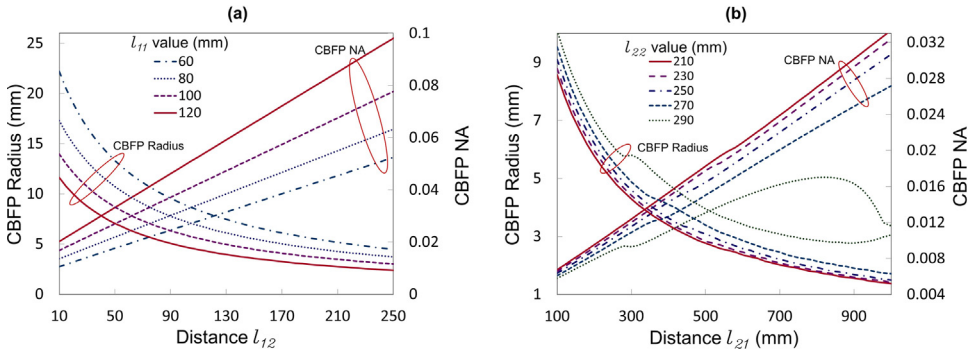

Fig. 7. Parametric fine adjustments for the angle-resolved illumination optics: (a) Lens group 1 and (b) Lens group 2.

Fig. 7 represents selected iteration process graphs of the parametric fine adjustments for the two Lens Groups with respect to the CBFP while maintaining appropriate telecentricity, showing that the radius and NA of the CBFP change with respect to the distances l_{11}, l_{12}, l_{21}, and l_{22}. The size and NA values change inversely each other with respect to these distances. The iterations are performed until the radii and NAs of the CBFP coincide for the two Lens Groups with the appropriate distance set.

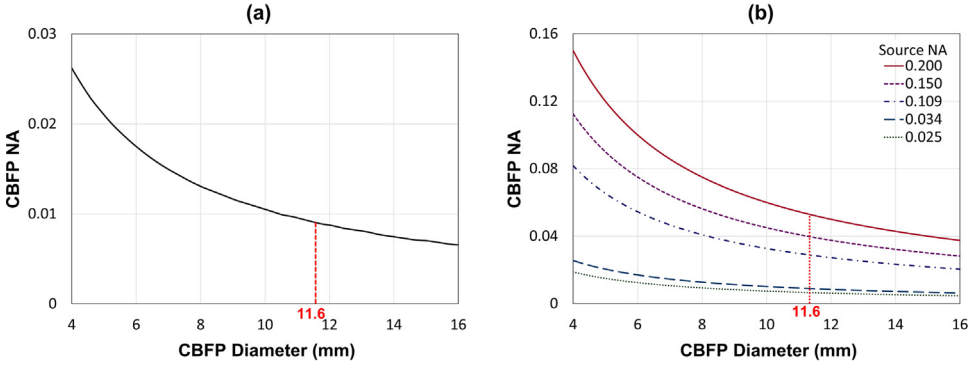

Fig. 8. Optimization of CBFP with respect to (a) Lens Group 2 and (b) Lens Group 1.

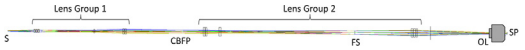

Fig. 9. Optimized angle-resolved illumination optics.

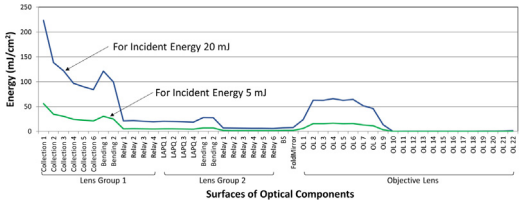

Fig. 10. Energy fluence of the designed 193 nm angle-resolved illumination optics.

Various NAs and diameters of the telecentric CBFP are obtained from multiple iterations with parametric adjustments of the Lens Groups as shown in Fig. 8. From Fig. 8(a) the NA and diameter of the CBFP for the Lens Group 2 are chosen to be 0.0085 and 11.6 mm, respectively, to have a CBFP large enough to resolve the illumination cone at the sample plane. The relationships between the NA and diameter of the CBFP for various configurations of the Lens Group 1 are shown in Fig. 8(b) yielding different source NAs while maintaining the diameter 3 mm. The source NA of 0.025 is matched to the values from Fig. 8(a) and the corresponding Lens Group 1 optics were chosen. With this combination, the source plane is transferred to the CBFP with a magnification of 3.86 times, forming a CBFP surface that has a large diameter to yield enough angle resolution of the illumination beams.

Fig. 9 is the bi-telecentric optics for angle-resolved illumination using a catadioptric objective lens designed by optimizing for relatively large CBFP.

5. Evaluation and discussion

The design of the angle-resolved bi-telecentric illumination optics is assessed numerically by evaluating fluence, aberrations, and wavefront homogeneity as functions of the illumination angle. The optimized illumination optics avoids any damaging concentration of the laser energy throughout the optical path. Using the specifications of the optical components such as transmittance and surface figures, the energy fluence is calculated for two input energies of 5.0 mJ and 20.0 mJ, which corresponds to the maximum energies of excimer lasers used to generate the angle-resolved illumination beams as shown in Fig. 10. The light travels through all components of the optics with only two elements exposed to a fluence as high as 22% of the nominal damage threshold.

The performance of the designed angle-resolved illumination optics depends on the quality of the CBFP, angular illumination beam at the sample plane, and the relationship between them. In accordance with the design criteria, therefore, the evaluation of the designed optics includes the characteristics of the telecentric CBFP and the wavefront deviations of the illumination beams at the sample plane.

The characteristics of the designed telecentric CBFP are arrayed in Fig. 11 for transverse ray aberrations, spot diagrams, field distortion, and telecentricity. Fig. 11(a) and (b) are transverse aberrations in tangential and sagittal ray fans with respect to source field positions, respectively, showing maximum deviation of ray propagation is less than 0.3 μm which meets the target specification in Table 1. The image transfer from the source plane to the CBFP is represented by the spot diagrams over the source height as shown in Fig. 11(c), showing maximum broadened spot at 0.5 μm with radius asymmetry of 0.8. The field distortion is less than 0.1% across the plane as the source is imaged onto the CBFP as shown in Fig. 11(d). Fig. 11(e) represents the telecentricity over the plane, which is defined as the chief ray parallelism over the optical plane, resulting in

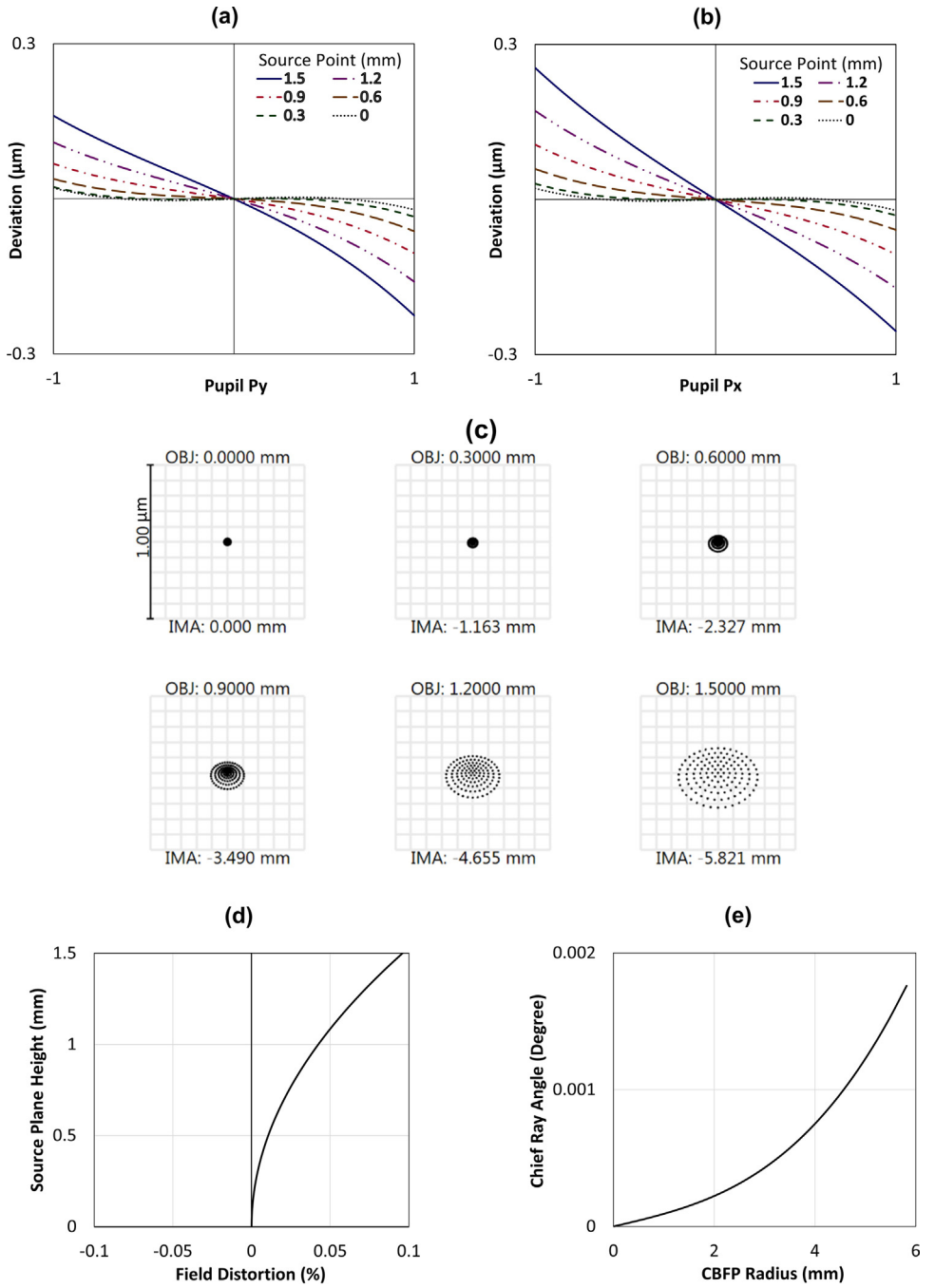

Fig. 11. Characteristics of the CBFP: (a), (b) transverse ray error for tangential and sagittal fans, (c) spot diagrams for source field position, (d) field distortion, and (e) chief ray parallelism.

less than 0.002° which is less than the target specification in Table 1 and is acceptable for performing CBFP scanning and engineering the angular illumination using the source unit scanning method as in Fig. 3(b).

Fig. 12(a) shows the conversion relationship of the illumination beam angle and NA at the sample plane to the CBFP position. The angle range of 7°–48° (NA = 0.12–0.74) corresponds to the CBFP position range of 0.95 mm–5.81 mm for this catadioptric objective lens, showing a highly linear relationship for NA and an illumination angle resolution of ΔNA = 0.0126 for an increment of 0.1 mm. Thus, these results demonstrate controllability of the conjugate back focal plane for engineering the angular illumination beam in the designed optics. Fig. 12(b) shows actual ray tracing at the CBFP and sample plane for

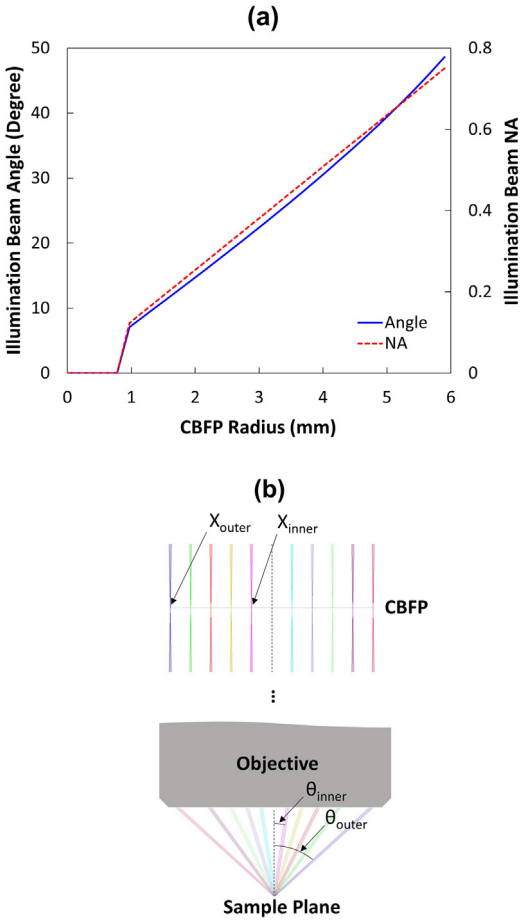

Fig. 12. Relationship of illumination beam angle and NA with respect to CBFP radius: (a) illumination beam angle and NA as a function of CBFP radius and (b) designed ray tracing at the CBFP and illumination sides.

discrete angle-resolved illumination beams using the designed optics, where θ_{inner} and θ_{outer} are the marginal inner and outer angles, which correspond to the marginal inner and outer positions at the CBFP, X_{inner} and X_{outer}, respectively.

For scatterfield microscopy, the wavefront quality of the angular illumination beam affects the scattered image signal in the microscope collection path, thus the evaluation of the illumination beams with respect to the CBFP is essential. As a commercial objective lens is used in the illumination optics, the designed illumination beam wavefronts are compared to the inherent illumination of the objective lens as the reference illumination.

The phase maps of the reference illumination and designed illumination of the marginal and central beams are shown in Fig. 13 for a field of view (FOV) of 78 μm. The central beam is limited to NA = 0.12 due to the central obscuration of the catadioptric objective lens. The reference illumination beams are obtained with ideal incident beams entering into the back focal plane (BFP) of the objective lens without the illumination optics, which means that the incident rays are from infinity. These reference beams, shown in Fig. 13(a) and (b), can be compared to the designed illumination beams that include the illumination optics, shown in Fig. 13(c) and (d). The peak-to-valley amplitude of the phase map is three times bigger for the designed illumination beams relative to the reference, but the root-mean-square (RMS) deviation values across the pupils are about 3% of the design wavelength (λ = 193.3 nm) and are within our acceptable error criteria. The actual field of view (FOV) at the sample plane will be about 30 μm in diameter due to the magnification and the charge-coupled device (CCD) size in the collection optical path. The actual size of the illumination area that affects the high-resolution image is about 40 μm or less and the pupil wavefront deviations are about 1% of the wavelength used. Having analyzed these initial wavefront deviations above, wavefront deviations are further evaluated for the two scanning methods: an aperture scan and an aperture source scan, as shown in Fig. 3. The first case includes the whole illumination optics, while the second case only requires Lens Group 2, and thus the wavefront deviation analysis for the Lens Group 2 is essential for both cases.

Fig. 14 is the wavefront evaluation results for Lens Group 2 with respective to illumination angle, wavelength, and the nominal linewidth of the 193-nm excimer laser. Wavefront error map with respect to the CBFP radius and wavelength ranging from 193.1 nm to 193.8 nm is shown in Fig. 14(a). Wavefront error variations over CBFP radius are relatively even,

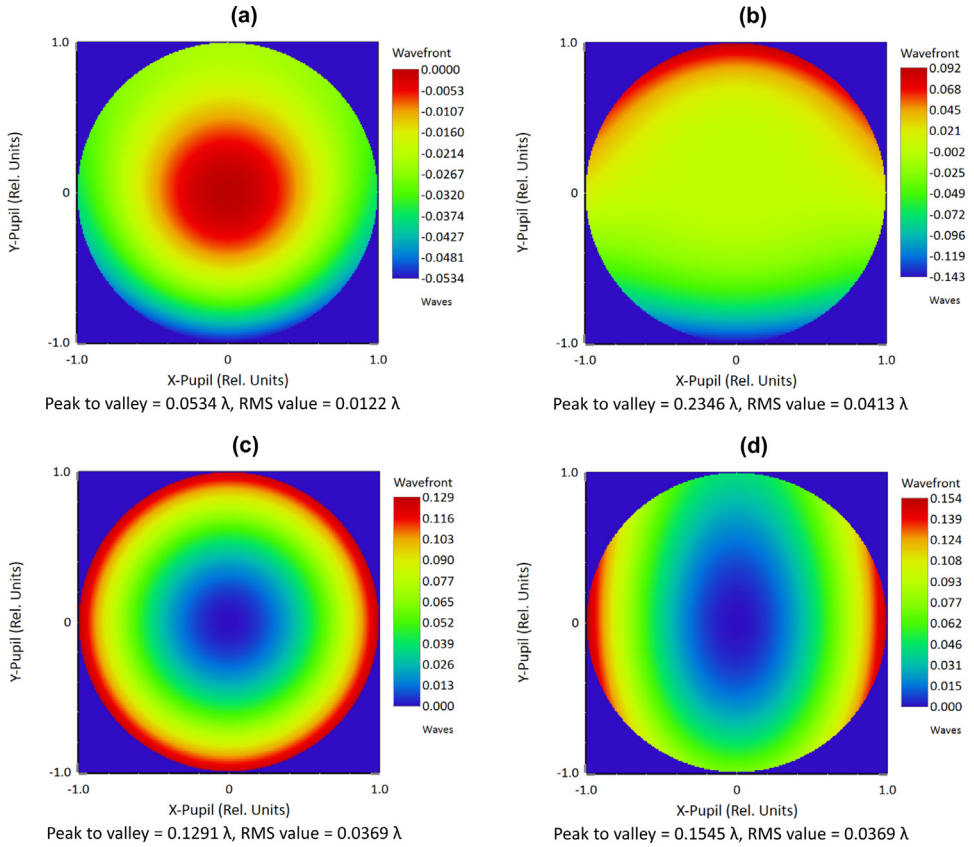

Fig. 13. Phase maps of reference and designed illumination beams. (a) Reference illumination for NA = 0.12, (b) reference illumination for NA = 0.74, (c) designed illumination for NA = 0.12, and (d) designed illumination for NA = 0.74.

while variations with respect to wavelength is relatively steep. Lowest wavefront errors of 0.3 λ or less are located between 193.4 nm and 193.5 nm. Based on this wavefront map, typical spectrum broadening of 193 nm excimer laser as in Fig. 14(b), in which central wavelength is 193.3 nm and FWHM (full width at half maximum) $\Delta\lambda = 0.3$ nm, is applied to yield an averaged wavefront error distribution by weighting 23 wavelength points within the broadened spectrum. Fig. 14(c) is the averaged wavefront error distribution over the illumination angle at the sample plane, showing maximum deviation of less than 0.06 λ with variation of 0.012 λ. The wavefront deviations for the broadened spectrum at a central wavelength of 193.3 nm are relatively constant for the illumination angle as well as are within the target specification in Table 1.

6. Conclusions

An angle-resolved Illumination optics for scatterfield microscopy using 193 nm excimer laser has been designed and optimized by adopting a nonimaging bi-telecentric system which features a telecentric CBFP as an object surface and a telecentric sample plane as a nonimaging surface. This optical configuration enables greater control of the angle-resolved illumination beam by establishing a relationship between the position within the CBFP and the illumination beam angle for two configurations: the aperture scan method in which an aperture at the CBFP is illuminated by a telecentric beam formed by preliminary relay optics and the source unit scan method in which a source unit is directly placed at the CBFP. Generalized methods applicable across wavelengths have been demonstrated for the design of non-imaging bi-telecentricity using two lens groups with respect to a CBFP. The designed optics has been evaluated numerically for angle-resolved illumination engineering capabilities with respect to aberrations for the CBFP and the illumination beams as design requirements. The feasibility of the bi-telecentric illumination optics is demonstrated by assessing the aberrations and telecentricity of CBFP, the relationship between the CBFP and the illumination beam angle, and the wavefront deviations of the angle-resolved illumination beams for an excimer laser linewidth. This optics will be used to obtain the angle-resolved illumination distribution maps that represent the tool-induced deviations including optical components and alignment errors, which are very useful for analysis and tailoring of scattered fields interacted with nanoscale features. This angle-resolved illumination optics holds promise for enabling the angle-resolved scatterfield microscopy for nanoscale features sized well-below the wavelength.

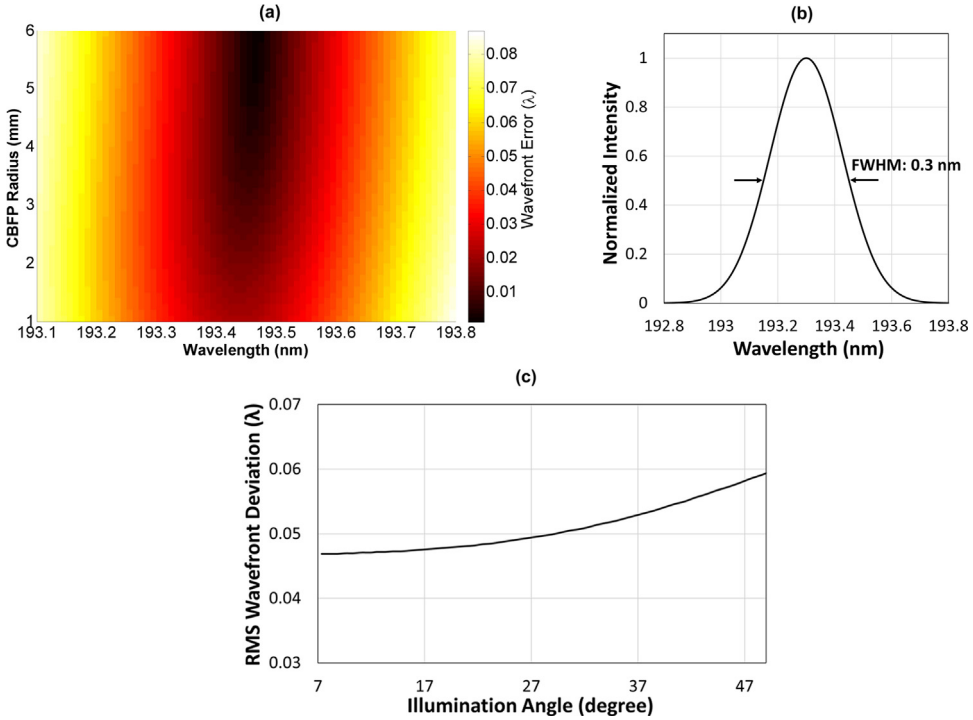

Fig. 14. RMS wavefront deviations of the angle-resolved illumination beams at the sample plane with respect to the CBFP: (a) RMS wavefront deviation map as the function of wavelength, (b) broadened spectrum of 193 nm excimer laser source, and (c) averaged RMS wavefront deviation using the source spectrum.

References

[1] R.M. Silver, B.M. Barnes, R. Attota, Scatterfield microscopy for extending the limits of image-based optical metrology, Appl. Opt. 46 (2007) 4248–4257, http://dx.doi.org/10.1364/AO.46.004248.
[2] R.M. Silver, B.M. Barnes, A. Heckert, R. Attota, R. Dixson, J. Jun, Angle resolved optical metrology, Proc. SPIE 6518 (2008) 69221M, http://dx.doi.org/10.1117/12.777131.
[3] B.M. Barnes, R. Attota, R. Quintanilha, Y. Sohn, R.M. Silver, Characterizing a scatterfield optical platform for semiconductor metrology, Meas. Sci. Technol. 22 (2011) 02403, http://dx.doi.org/10.1088/0957-0233/22/2/024003.
[4] M.H. Madsen, P.-E. Hansen, Imaging scatterometry for flexible measurements of patterned areas, Opt. Express 24 (2016) 254208, http://dx.doi.org/10.1364/OE.24.001109.
[5] J. Qin, R.M. Silver, B.M. Barnes, H. Zhou, R.G. Dixson, M.A. Henn, Deep-subwavelength nanometric image reconstruction using Fourier domain optical normalization, Light Sci. Appl. 5 (2016) e16038, http://dx.doi.org/10.1038/lsa.2016.38.
[6] B.M. Barnes, M.-A. Henn, M.Y. Sohn, H. Zhou, R.M. Silver, Enabling quantitative optical imaging for in-die-capable critical dimension targets, Proc. SPIE 9778 (2016) 97789Y, http://dx.doi.org/10.1117/12.2221920.
[7] B.M. Barnes, M.Y. Sohn, F. Goasmat, H. Zhou, A.E. Vladar, R.M. Silver, A. Arceo, Three-dimensional deep sub-wavelength defect detection using lambda = 193 nm optical microscopy, Opt. Express 21 (2013) 26219–26226, http://dx.doi.org/10.1364/OE.21.026219.
[8] A.M.H. Wong, G.V. Eleftheriades, An optical super-microscope for far-field, real-time imaging beyond the diffraction limit, Sci. Rep. 3 (2013) 1715, http://dx.doi.org/10.1038/srep01715.
[9] J. Qin, R.M. Silver, B.M. Barnes, H. Zhou, F. Goasmat, Fourier domain optical tool normalization for quantitative parametric image reconstruction, Appl. Opt. 52 (2013) 6512–6522, http://dx.doi.org/10.1364/AO.52.006512.
[10] M.Y. Sohn, B.M. Barnes, H. Zhou, R.M. Silver, Quantitative tool characterization of 193nm scatterfield microscope, Proc. SPIE 9556 (2015) 955611, http://dx.doi.org/10.1117/12.2188224.
[11] A. Koehler, New method of illumination for photomicrographical purposes, J. R. Microsc. Soc. 14 (1894) 261–262, http://dx.doi.org/10.1111/j.1365-2818.1894.tb00027.x.
[12] L.C. Martin, London, in: The Theory of the Microscope, Blackie & Son, 1966 http://trove.nla.gov.au/version/45463882.
[13] Z. Kam, M.L. Jones, H. Chen, D.A. Agard, J.W. Sedat, Design and construction of an optimal illumination system for quantitative wide-field multi-dimensional microscopy, Bioimaging 1 (1993) 71–81 http://onlinelibrary.wiley.com/doi/10.1002/1361-6374(199306)1:2%3C71::AID-BIO2%3E3.0.CO;2-%23/abstract.
[14] G. Benner, W. Probst, Köhler illumination in the TEM: fundamentals and advantages, J. Microsc. 174 (1994) 133–142, http://dx.doi.org/10.1111/j.1365-2818.1994.tb03461.x.
[15] A. Laskin, P. Kaiser, V. Laskin, A. Ostrun, Laser beam shaping for biomedical microscopy techniques, Proc. SPIE 9887 (2016) 98872E, http://dx.doi.org/10.1117/12.2217927.
[16] M.A. Pate, Optical design and specification of telecentric optical systems, Proc. SPIE 3482 (1998) 877–886, http://dx.doi.org/10.1117/12.322029.
[17] C. Hammond, A symmetrical representation of the geometrical optics of the light microscope, J. Microsc. 192 (1998) 63–68, http://dx.doi.org/10.1046/j.1365-2818.1998.00408.x.
[18] G.I. Greisukh, E.G. Ezhov, I.A. Levin, S.A. Stepanov, Design of the double-telecentric high-aperture diffractive-refractive objectives, Appl. Opt. 50 (2011) 3254–3258, http://dx.doi.org/10.1364/AO.50.003254.
[19] J. Chaves, Boca Raton, in: Introduction to Nonimaging Optics, 2nd edition, CRC Press, 2016, http://dx.doi.org/10.1201/b18785.
[20] D. Meng, X. Yang, T. Jian, L. Qi, The design of double telecentric lens with large aperture based on machine vision, Proc. SPIE 9297 (2014) 929719, http://dx.doi.org/10.1117/12.2072439.

[21] J. Zhang, X. Chen, J. Xi, Z. Wu, Paraxial analysis of double-sided telecentric zoom lenses with four components, Opt. Eng. 53 (2014) 115103, http://dx.doi.org/10.1117/1.OE.53.11.115103.
[22] M.Y. Sohn, R.M. Silver, 193 nm scatterfield microscope illumination optics, SPIE 9293 (2014) 92931D, http://dx.doi.org/10.1117/12.2074211.
[23] P.M. Schermerhorn, Excimer laser damage testing of optical materials, Proc. SPIE 1835 (1992) 70–79, http://dx.doi.org/10.1117/12.143031.
[24] G.H. Seward, Optical Design of Microscopes, SPIE Press, Bellingham, 2010, http://dx.doi.org/10.1117/3.855480.
[25] J.C. Wyant, K. Creath, J.C. Wyant, Basic wavefront aberration theory for optical metrology, in: R.R. Shannon (Ed.), Applied Optics and Optical Engineering, vol. XI, Academic Press, New York, 1992, p. 39.
[26] R.R. Shannon, The Art and Science of Optical Design, Cambridge University Press, 1997, pp. 323, http://dx.doi.org/10.1017/CBO9780511816529.
[27] M. Born, E. Wolf, Principles of Optics, 7th ed., Cambridge University Press, Cambridge, 1999, pp. 528, http://dx.doi.org/10.1017/CBO9781139644181.